

# Camera-based 3D Semantic Scene Completion with Sparse Guidance Network

Jianbiao Mei<sup>1</sup>, Yu Yang<sup>1</sup>, Mengmeng Wang<sup>1</sup>, Junyu Zhu<sup>1</sup>, Xiangrui Zhao<sup>1</sup>, Jongwon Ra<sup>1</sup>,  
Laijian Li<sup>1</sup>, Yong Liu<sup>1\*</sup>

<sup>1</sup>Institute of Cyber-Systems and Control, Zhejiang University  
{jianbiaomei, yu.yang, mengmengwang, junyuzhu, xiangruizhao, jongwonra, lilaijian}@zju.edu.cn;  
yongliu@ipc.zju.edu.cn

## Abstract

Semantic scene completion (SSC) aims to predict the semantic occupancy of each voxel in the entire 3D scene from limited observations, which is an emerging and critical task for autonomous driving. Recently, many studies have turned to camera-based SSC solutions due to the richer visual cues and cost-effectiveness of cameras. However, existing methods usually rely on sophisticated and heavy 3D models to directly process the lifted 3D features that are not discriminative enough for clear segmentation boundaries. In this paper, we adopt the dense-sparse-dense design and propose an end-to-end camera-based SSC framework, termed SGN, to diffuse semantics from the semantic- and occupancy-aware seed voxels to the whole scene based on geometry prior and occupancy information. By designing hybrid guidance (sparse semantic and geometry guidance) and effective voxel aggregation for spatial occupancy and geometry priors, we enhance the feature separation between different categories and expedite the convergence of semantic diffusion. Extensive experimental results on the SemanticKITTI dataset demonstrate the superiority of our SGN over existing state-of-the-art methods. Code is available at <https://github.com/Jieqianyu/SGN>.

## Introduction

3D scene understanding constitutes the bedrock of autonomous driving systems. By precisely perceiving the occupancy and semantics of their surroundings, autonomous vehicles can make informed decisions and navigate safely. To this end, Semantic Scene Completion (SSC) has been introduced to predict the semantic occupancy of each voxel of the entire 3D scene from limited observation. However, accurately estimating the semantics and geometry of the real world from partial observations is challenging due to the complexities presented by real-world scenarios.

SSC has attracted extensive studies due to its application prospects for downstream tasks such as mapping and planning. When working with outdoor driving scenes, LiDAR has emerged as a popular input modality for many existing methods (Roldão, de Charette, and Verroust-Blondet 2020; Cheng et al. 2021; Rist et al. 2021; Yan et al. 2021; Xia et al. 2023; Li et al. 2023b) to capture 3D information of surroundings, but it suffers from high-cost sensors. Recently, there has been a shift towards camera-based SSC solutions. As the

\*Corresponding author

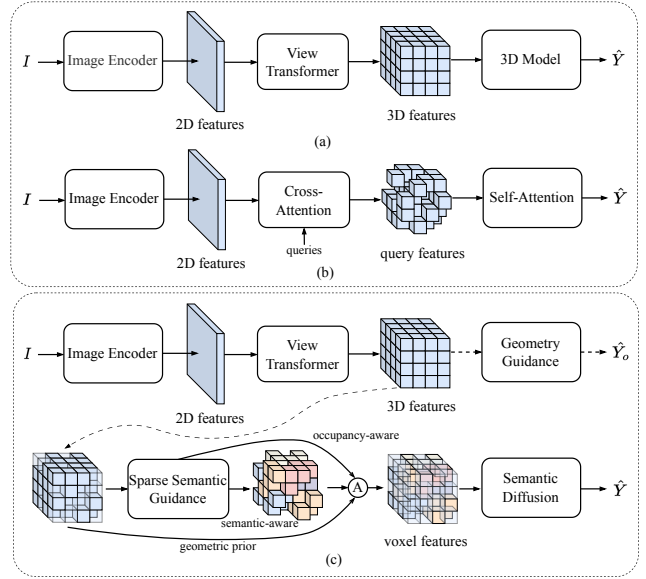


Figure 1: (a) Fully dense processing with heavy and complex 3D model. (b) MAE-like architecture in a “sparse-to-dense” manner. (c) Our “dense-sparse-dense” design with hybrid guidance and semantic diffusion.

pioneer, MonoScene (Cao and de Charette 2022) proposed the first framework for monocular 3D SSC, utilizing mapping projection to lift RGB images to 3D volumes processed with the 3D UNet. Afterward, many camera-based methods such as OccDepth (Miao et al. 2023), SurroundOcc (Wei et al. 2023), and OccFormer (Zhang, Zhu, and Du 2023) are developed with a similar pipeline consisting of the image backbone, view transformer, and 3D model, as illustrated in Fig.1 (a). However, they rely on sophisticated and heavy 3D models to directly process the lifted 3D features that are not discriminative enough for clear segmentation boundaries. We explain that the lifted 3D features by 3D-2D mapping projection (Cao and de Charette 2022) contain many ambiguities due to the assumption of the uniform depth distribution and 2D-3D methods such as LSS (Pillion and Fidler 2020) only utilize coarse surface information from depth distribution estimation.

On the other hand, VoxFormer (Li et al. 2023d) proposed an MAE-like architecture to complete non-visible structures using constructed visible areas. It adopts the two-stage framework, with the first stage for query proposal and the second stage for densification and segmentation. By completing the 3D scene in a **sparse-to-dense** manner shown in Fig.1 (b), VoxFormer is more efficient and scalable than the dense processing with heavy 3D models mentioned above. However, it still suffers from several limitations. Firstly, the densification stage is mainly considered from the perspective of scene completion based on queries. The intra-category feature separation of queries is neglected. Besides, the second stage only considers the information from the queries that only include partial observation and are not always accurate, increasing the difficulty of subsequent completion and segmentation. Finally, the two-stage training and inference cannot fully consider global information due to the independent optimization of different stages. The spatial occupancy information from the first stage is also not fully utilized.

To address the above problems, we propose a novel end-to-end camera-based SSC framework, **Sparse Guidance Network (SGN)**, to diffuse semantics from the semantic- and occupancy-aware seed voxels to the whole scene based on geometry prior and occupancy information, as illustrated in Fig.1 (c). Specifically, we employ the **dense-sparse-dense** design to implement the semantic diffusion of seed features, avoiding relying on heavy 3D models to process coarse scene representations that are not discriminative enough. Firstly, to dynamically select sparse seed voxels and provide occupancy-aware information, we redesign the sparse voxel proposal network to directly process points generated by depth prediction with the coarse-to-fine paradigm. And by further designing hybrid guidance (sparse semantic and geometry guidance) and effective voxel aggregation for spatial occupancy and geometry priors, we enhance the intra-category feature separation and expedite the convergence of the semantic diffusion. We also devise the multi-scale semantic diffusion module using anisotropic convolutions (Li et al. 2020) for flexible receptive field while reducing the computation resources. By this means, our end-to-end SGN is lightweight while having a more powerful representation ability.

Extensive experiments on the challenging SemanticKITTI dataset (Behley et al. 2019) demonstrate the superiority of our SGN over existing state-of-the-art methods. For example, on the validation set, even our light version SGN-L achieves notable scores of 14.80% mIoU and 45.45% IoU with only **12.5 M** parameters and **7.16 G** memory for training, exceeding VoxFormer-T by 1.45% points in mIoU and 1.30% points in IoU while being more lightweight and less memory consumption.

Our main contributions can be summarized as follows:

- We propose an end-to-end camera-based SSC framework called **SGN**, propagating semantics from the semantic- and occupancy-aware seed voxels to the whole scene based on geometry prior and occupancy information.
- We adopt the **dense-sparse-dense** design and propose hybrid guidance and effective voxel aggregation to enhance intra-categories feature separation and expedite the

convergence of the semantic diffusion.

- Extensive experiments on the SemanticKITTI benchmark demonstrate the effectiveness of our SGN, which is more lightweight and achieves the new state-of-the-art.

## Related Works

**Semantic Scene Completion.** Due to the vital application of semantic occupancy prediction in autonomous driving, SSC has attracted extensive attention. After the release of the large-scale outdoor benchmark SemanticKITTI (Behley et al. 2019), many outdoor SSC methods have emerged. According to the input modality, existing outdoor methods can be mainly classified into LiDAR-based and camera-based methods. LiDAR-based methods consider LiDAR a primary modality to enable accurate 3D semantic occupancy prediction. Following the pioneering SSCNet (Song et al. 2017), U-Net (Zou et al. 2021) exploits a single 3D U-Net framework to obtain predictions from the grids generated by the LiDAR points, resulting in extra computation overhead of empty voxels. Afterward, LMSCNet (Roldão, de Charette, and Verroust-Blondet 2020) introduces the 2D CNN for feature encoding, and SGCNet (Zhang et al. 2018) uses spatial group convolutions to improve efficiency. Some solutions focus on multi-view fusion (Cheng et al. 2021), local implicit functions (Rist et al. 2021), and knowledge distillation (Xia et al. 2023) for SSC. Besides, the relationships between semantic segmentation and scene completion are explored. For example, JS3C-Net (Yan et al. 2021) and SSA-SC (Yang et al. 2021) design a semantic segmentation network to assist the semantic scene completion. SSC-RS (Mei et al. 2023) design multi-branch network to fuse semantic and geometry features hierarchically.

Recently, camera-based perception such as detection (Huang et al. 2021; Wang et al. 2022; Liu et al. 2022; Li et al. 2022; Wang et al. 2021; Chen et al. 2022b) and segmentation (Li et al. 2022; Zhou and Krähenbühl 2022; Chen et al. 2022a) is currently more attractive due to cameras' richer visual cues and cost-effectiveness. And there is also a shift towards camera-based solutions (Cao and de Charette 2022; Huang et al. 2023) to SSC. MonoScene (Cao and de Charette 2022) first proposed to infer 3D SSC from a single monocular RGB image, which applied a classical 3D UNet network to process the voxel features projected along the line of sight. Afterward, TPVFormer (Huang et al. 2023) proposed a tri-perspective view (TPV) representation to describe the fine-grained 3D structure of a scene. VoxFormer (Li et al. 2023d) proposed an MAE-like architecture to complete non-visible structures using constructed visible areas. OccFormer (Zhang, Zhu, and Du 2023) designed a dual-path transformer network. And SurroundOcc (Wei et al. 2023) applied 3D convolutions to upsample multi-scale voxel features progressively and devised a pipeline to generate dense SSC ground truth. Symphonize (Jiang et al. 2023) modeled the scene volume with a sparse set of instance queries with context awareness. Some methods (Miao et al. 2023; Li et al. 2023a) leveraged implicit stereo depth information and stereo matching to resolve geometry ambiguity. Besides, there are some SSC solutions (Huang et al. 2023; Wei et al. 2023; Gan

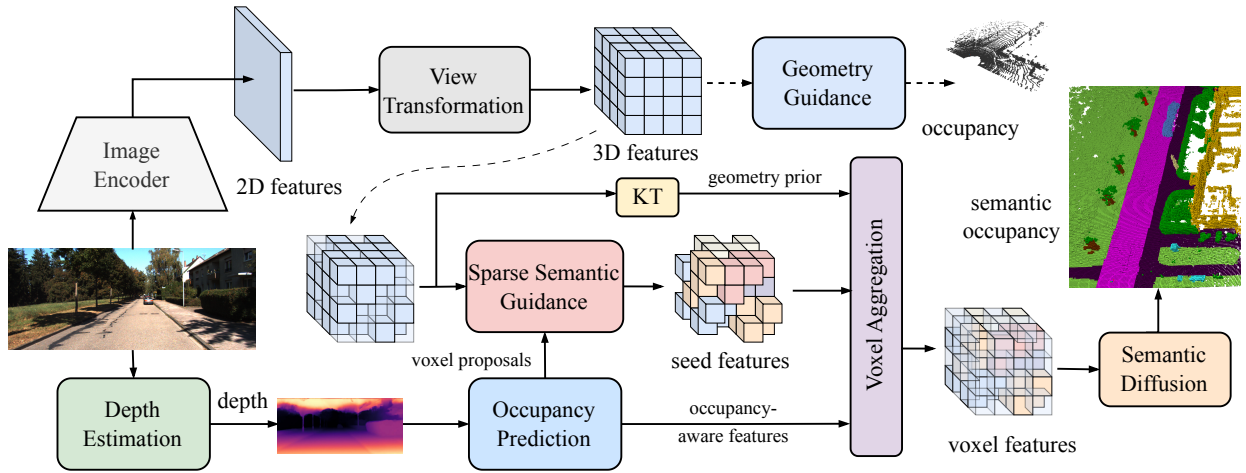


Figure 2: Overall framework of our SGN. The image encoder extracts 2D features to provide the foundation for 3D features lifted by the view transformation. Then auxiliary occupancy head is applied to provide geometry guidance. Before sparse semantic guidance, depth-based occupancy prediction is utilized for voxel proposals of indexing seed features. Afterward, the voxel aggregation layer forms the informative voxel features processed by the multi-scale semantic diffusion for the final semantic occupancy prediction. KT denotes the knowledge transfer layer for geometry prior.

et al. 2023; Li et al. 2023e) for multi-view cameras. And multiple benchmarks (Li et al. 2023c; Tian et al. 2023; Wang et al. 2023) are proposed to facilitate the SSC’s development.

We focus on camera-based SSC in outdoor scenarios. Compared with the existing works, our SGN proposes to diffuse semantics from the semantic- and occupancy-aware seed voxels to the whole scene based on the geometry prior and occupancy information. SGN avoids relying on heavy and sophisticated 3D models to handle lifted voxel features with rough geometry context like many existing SSC methods (Cao and de Charette 2022; Wei et al. 2023; Zhang, Zhu, and Du 2023; Miao et al. 2023; Jiang et al. 2023). Our method is built on the recent two-stage method VoxFormer (Li et al. 2023d). However, unlike VoxFormer, our SGN is end-to-end, which adopts the dense-sparse-dense design and proposes hybrid guidance and effective voxel aggregation to enhance intra-categories feature separation and expedite the convergence of the semantic diffusion. Compared with VoxFormer, our SGN achieved better performance while being more lightweight and requiring less memory consumption.

## Method

### Overview

We show the overall framework of our SGN in Fig.2. SGN adopts the dense-sparse-dense design and propagates semantics from the semantic- and occupancy-aware seed voxels to the whole scene based on geometry prior and occupancy information. SGN takes RGB images as the input and extracts 2D features using the image encoder. Then the 3D features are obtained through the view transformation. For dynamically indexing the seed voxels, we generate the sparse voxel proposals based on depth prediction. Then according to the voxel proposals and 3D features, the hybrid guidance is designed to inject semantic and geometry cues and facilitate

feature learning. Furthermore, we develop the voxel aggregation layer to form the informative voxel features, which are further processed by our multi-scale semantic diffusion module for the final semantic occupancy prediction.

**Image Encoder.** We use ResNet-50 (He et al. 2016) with FPN (Lin et al. 2017) to construct the image encoder for extracting 2D features from RGB images. The extracted features  $\mathbf{F}^{2D} \in \mathbb{R}^{N_t \times C \times H \times W}$  provide a strong foundation for the subsequent voxel features, where  $N_t$  is the image number of temporal inputs,  $C$  is the feature channel and  $(H, W)$  denotes the image resolution.

**View Transformation.** Similar to MonoScene (Cao and de Charette 2022), we construct 3D features by sampling 2D features via 3D-2D projection mapping with camera parameters. The simple projection mapping operation provides coarse volumetric scene representation for the latter contextual modeling. And it is more convenient and concise than learnable LSS (Phillion and Fidler 2020) and cross-attention mechanism (Li et al. 2022).

Let  $\mathbf{x} \in \mathbb{R}^{X \times Y \times Z \times 3}$  denote the centroid of  $X \times Y \times Z$  voxels in world coordinates. We establish the projection mapping  $\pi(\mathbf{x})$  using the camera parameters  $(K, T)$ , where  $K$  and  $T$  are the cameras intrinsic and extrinsic matrices directly provided in KITTI (Geiger, Lenz, and Urtasun 2012). We take the average of sampled features from different images for each voxel. And the features of voxels outside the field of view (FOV) are set to zero. Mathematically, the 3D features  $\mathbf{F}^{3D} \in \mathbb{R}^{C \times X \times Y \times Z}$  are sampled from the 2D features  $\mathbf{F}^{2D}$  as follows:

$$\mathbf{F}^{3D} = W \cdot \sum_{t=1}^{N_t} [\phi_{\pi(\mathbf{x})}(\mathbf{F}_t^{2D}) \cdot M_t^{FOV}] \quad (1)$$

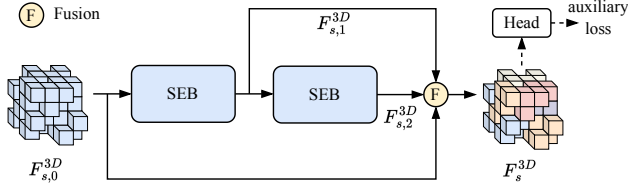


Figure 3: Detailed architecture of the proposed semantic guidance module. Sparse encoder block (SEB) consists of a sparse feature encoder and a sparse geometry feature encoder adopted from (Ye et al. 2022).

$$W_p = \begin{cases} 1/\delta_p, & \delta_p > 0, \\ 1, & \delta_p = 0. \end{cases} \quad (2)$$

where  $\phi_a(b)$  is the sampling function that samples features  $b$  at coordinates  $a$ ,  $\mathbf{F}_t^{2D}$  is the 2D features of image  $\mathbf{I}_t$ ,  $M_t^{FOV} \in \mathbb{R}^{1 \times H \times W}$  is the binary mask indicating the field of view of image  $\mathbf{I}_t$ ,  $\delta_p$  is the number of hit images for point  $p$  in  $\mathbf{x}$ ,  $W_p$  is the weight value for points  $p$  in  $W$ .

### Feature Learning with Hybrid Guidance

As discussed above, most existing methods design heavy models to directly process the 3D features  $\mathbf{F}^{3D}$  produced by the view transformation module for the final semantic scene prediction. We argue that the coarse scene representation  $\mathbf{F}^{3D}$  is not discriminative enough to get clear segmentation boundaries, which slows down the convergence of the model. Therefore, we propose sparse semantic guidance and geometry guidance to inject semantic and geometry cues for informative voxel features.

**Geometry Guidance.** We first attach the auxiliary 3D occupancy head as the geometry guidance after the 3D features from the view transformation module to provide coarse geometry awareness. Specifically, we construct the 3D occupancy head with an anisotropic convolution layer (Li et al. 2020) and a linear layer. In the spirit of (Zhou et al. 2020), the anisotropic convolution decomposes a 3D convolution operation into three consecutive 1D convolutions in different directions. Additionally, each of these 1D convolutions is equipped with a mixer containing distinct kernel sizes, enhancing the model’s ability to learn and extract meaningful features from the input data. It can provide flexible receptive fields while alleviating resource consumption. By predicting the 3D occupancy  $\hat{\mathbf{Y}}_o$  on the lifted 3D features  $\mathbf{F}^{3D}$  using the auxiliary head, we apply the guidance on the coarse scene representation and provide the geometry prior for the latter seed features’ semantic prediction and diffusion. We optimize the occupancy probability with binary cross-entropy loss:

$$\mathcal{L}_{geo} = - \sum_i [(1 - \mathbf{Y}_{o,i}) \log(1 - \hat{\mathbf{Y}}_{o,i}) + \mathbf{Y}_{o,i} \log(\hat{\mathbf{Y}}_{o,i})] \quad (3)$$

where  $i$  indexes the voxel of the 3D scene and  $\mathbf{Y}_o$  is the occupancy ground truth. Note that the auxiliary 3D head is abandoned during inference and using geometry guidance does not introduce any extra computation.

**Sparse Semantic Guidance.** Since directly learning the semantics of all the voxels from the 3D features with coarse volumetric information is less effective and efficient, we propose propagating **semantics** from **seed** voxel to the whole scene. Specifically, we generate sparse voxel proposals to choose seed voxels and encourage inter-category separability of seed features with semantic guidance, expediting the latter semantic diffusion.

**Sparse Voxel Proposal.** We devise the sparse voxel proposal network (SVPN) to generate sparse proposals for indexing seed voxels. Unlike Voxformer (Li et al. 2023d), which learns class-agnostic proposals on temporal data **offline** for voxel queries, our SVPN aims to dynamically select seed voxels **online** by occupancy probability for subsequent semantic context learning. Specifically, SVPN consists of depth estimation and coarse-to-fine occupancy prediction. Following (Li et al. 2023d; Jiang et al. 2023), we utilize the pre-trained MobileStereoNet (Shamsafar et al. 2022) to infer the depth prediction and calculate the scene points  $\mathbf{P}$  by back-projecting the depth map into the 3D point cloud using the camera parameters  $(K, T)$ . The scene points  $\mathbf{P}$  imply the volumetric surface and are used for occupancy prediction.

Next, we generate the occupancy prediction  $\mathbf{O} \in \mathbb{R}^{X \times Y \times Z}$  in a coarse-to-fine manner. Firstly, the points  $\mathbf{P}$  are fed into a voxelization layer adopted from DRNet (Ye et al. 2021) for voxel-wise features. Then we apply the tiny sparse convolution network consisting of a sparse feature encoder and a sparse geometry feature encoder adopted from GASN (Ye et al. 2022) to predict the coarse occupancy probability from the voxel-wise features. Finally, the occupancy probability is further fed into a lightweight Unet-like network (Roldão, de Charette, and Verroust-Blondet 2020) for the final occupancy prediction  $\mathbf{O}$ , which is used to select the sparse voxels as explained in semantic guidance. Similar to the geometry guidance, we use the binary cross entropy loss to calculate the loss  $\mathcal{L}_{occ}$  for occupancy prediction.

To utilize the occupancy-aware cues, we also take the 3D features  $\mathbf{F}_o^{3D} \in \mathbb{R}^{C_o \times X \times Y \times Z}$  from the last layer of the Unet-like network for the latter voxel feature aggregation.

**Semantic Guidance.** After obtaining the occupancy prediction  $\mathbf{O}$  and voxel coordinates  $V^{3D} \in \mathbb{Z}^{3 \times X \times Y \times Z}$  of the scene, we first choose the initial seed voxel features  $\mathbf{F}_{s,0}^{3D} \in \mathbb{R}^{C \times N_s}$  and seed coordinates  $V_s^{3D} \in \mathbb{Z}^{3 \times N_s}$  by:

$$V_s^{3D} = V^{3D}[:, \mathbf{O} > \theta] \quad (4)$$

$$\mathbf{F}_{s,0}^{3D} = \mathbf{F}^{3D}[:, \mathbf{O} > \theta] \quad (5)$$

where  $\theta$  is the threshold to determine if the voxel is occupied and  $N_s$  is the number of non-empty voxel. Then these seed voxel features  $\mathbf{F}_{s,0}^{3D}$  and corresponding voxel indices  $V_s^{3D}$  are fed into the semantic guidance module illustrated in Fig.3 for mutual interactions. The semantic guidance module has two sparse encoder blocks (SEB), a fusion layer, and an auxiliary semantic head. Each encoder block consists of a sparse feature encoder and a sparse geometry feature encoder adopted from (Ye et al. 2022) and outputs features with multi-scale contextual information. Let  $\mathbf{F}_{s,1}^{3D}, \mathbf{F}_{s,2}^{3D}$  are the outputs

of the two sparse encoder blocks, the fusion feature  $\mathbf{F}_s^{3D} \in \mathbb{R}^{C \times N_s}$  are obtained by:

$$\mathbf{F}_s^{3D} = \text{MLP}([\mathbf{F}_{s,0}^{3D}, \mathbf{F}_{s,1}^{3D}, \mathbf{F}_{s,2}^{3D}]) \quad (6)$$

where  $[\cdot]$  denotes concatenate operation along feature dimension. After that, the fused features  $\mathbf{F}_s^{3D}$  are fed into the auxiliary semantic head consisting of a two-layer MLP to predict the corresponding semantics  $\hat{\mathbf{Y}}_s \in \mathbb{R}^{C_{class} \times N_s}$ , where  $C_{class}$  is the number of classes. We calculate the cross entropy loss and lovasz loss (Berman, Rannen Triki, and Blaschko 2018) for the semantic guidance:

$$\mathcal{L}_{sem} = \mathcal{L}_{ce}(\hat{\mathbf{Y}}_s, \mathbf{Y}_s) + \mathcal{L}_{lovasz}(\hat{\mathbf{Y}}_s, \mathbf{Y}_s) \quad (7)$$

where  $\mathbf{Y}_s$  is the seed voxels’ semantic label indexed from the semantic scene label  $\mathbf{Y}$ .

By this means, we inject semantic cues into the fused seed features  $\mathbf{F}_s^{3D}$  and enhance the feature separation between categories, which is the key to semantic diffusion.

**Voxel Aggregation.** As shown in Fig.2, we further aggregate the semantic-aware seed features  $\mathbf{F}_s^{3D}$  and occupancy-aware features  $\mathbf{F}_o^{3D}$  with 3D features  $\mathbf{F}^{3D}$  implying coarse geometry representation to construct the final discriminative voxel features  $\mathbf{F}_f^{3D} \in \mathbb{R}^{(C+C_o) \times X \times Y \times Z}$ . Specifically, we leverage the coordinates of non-seed voxels to index features  $\mathbf{F}_n^{3D}$  from  $\mathbf{F}^{3D}$ . Then the non-seed voxel features  $\mathbf{F}_n^{3D}$  are fed into a knowledge transfer layer and combined with the semantic-aware features  $\mathbf{F}_s^{3D}$  to form the new scene representation, which contains the semantic context and geometry prior. We argue that non-seed voxel features  $\mathbf{F}_n^{3D}$  are vital and can well complement the seed features since the sparse voxel proposals are not always accurate. To exploit spatial occupancy information from the SVPN, we also concatenate the occupancy-aware features  $\mathbf{F}_o^{3D}$  with the new scene representation to obtain the final voxel features. The detailed procedure can be formulated as follows:

$$\mathbf{F}_f^{3D} = \text{MLP}([\text{CN}(\mathbf{F}_s^{3D}, \text{KT}(\mathbf{F}_n^{3D})), \mathbf{F}_o^{3D}]) \quad (8)$$

where CN is the feature combination of seed and non-seed voxels, and KT is the linear layer for knowledge transfer.

### Multi-Scale Semantic Diffusion

By learning features with hybrid guidance, we obtain discriminative voxel features with rich semantic context and spatial geometry cues. Then we design the multi-scale semantic diffusion (MSSD) module to propagate the semantic information from seed features to the whole scene based on the geometry and spatial occupancy cues. The MSSD module contains three anisotropic convolution layers (Li et al. 2020) and the ASPP module, which is lightweight while well capturing multi-scale features for instances with different sizes. Afterward, we use the head consisting of a linear layer and softmax layer to predict the final semantic scene prediction  $\hat{\mathbf{Y}} \in \mathbb{R}^{C_{class} \times X \times Y \times Z}$  from the diffused voxel features.

Following MonoScene (Cao and de Charette 2022), we adopt the Scene-Class Affinity Loss on both semantic and geometry results of  $\hat{\mathbf{Y}}$  to optimize the class-wise derivable

precision, recall, and specificity metrics simultaneously. The overall loss function for the final prediction is formulated by:

$$\mathcal{L}_{ssc} = \mathcal{L}_{scal}^{sem}(\hat{\mathbf{Y}}, \mathbf{Y}) + \mathcal{L}_{scal}^{geo}(\hat{\mathbf{Y}}, \mathbf{Y}) + \mathcal{L}_{ce}(\hat{\mathbf{Y}}, \mathbf{Y}) \quad (9)$$

### Training Loss

Unlike VoxFormer (Li et al. 2023d) with sophisticated two-stage training, we train our SGN end-to-end. The total training loss  $\mathcal{L} = \mathcal{L}_{geo} + \mathcal{L}_{occ} + \mathcal{L}_{sem} + \mathcal{L}_{ssc}$ .

## Experiments

To evaluate our SGN, we conduct extensive experiments on the challenging large-scale outdoor dataset SemanticKITTI (Behley et al. 2019). Due to the page limitation, more details on the datasets, metrics, experiments, and qualitative results are provided in the supplementary materials.

### Implementation Details

We crop the input RGB images of cam2 to size  $1220 \times 370$  and take the 2D feature map with 1/16 of the input resolution. The feature dimension  $C$  and the channel number  $C_o$  are set to 128 and 8, respectively. The size  $X \times Y \times Z$  of the 3D feature volume is  $128 \times 128 \times 16$ . And the final predictions are up-sampled to  $256 \times 256 \times 32$ . The threshold  $\theta$  for selecting seed voxels is set to 0.5 by default. We train SGN for 40 epochs on 4 V100 GPUs with a total batch size of 4. The AdamW (Loshchilov and Hutter 2017) optimizer is used with an initial learning rate of  $2e-4$  and a weight decay of  $1e-2$ . Following VoxFormer (Li et al. 2023d), we design the single-image version SGN-S, taking only the current image as input and the temporal version SGN-T with the current and the previous 4 images as input. We also provide the light temporal version SGN-L, which takes temporal inputs and uses ResNet18 as the backbone with dimension  $C = 64$  and 1 anisotropic convolution layer for MSSD.

### Comparison with the state-of-the-art

Table 1 and Table 2 present the comparison results between our SGN and other state-of-the-art camera-based SSC methods on the SemanticKITTI validation and test sets, respectively. Our SGN-T achieves state-of-the-art performance on both SemanticKITTI validation and test sets. Specifically, SGN-T outperforms the second one by 1.86% points (OccFormer) and 2.19% points (VoxFormer) regarding mIoU and IoU, as shown in Table 2. And compared with these fully dense processing methods with complex 3D models, such as MonoScene, OccFormer, and Symphonize, our SGN-S also performs better in terms of mIoU and IoU. For example, SGN-S greatly boosts the MonoScene by 3.47% points in mIoU and 6.74% points in IoU, demonstrating the effectiveness of our dense-sparse-dense design equipped with hybrid guidance. Notably, SGN-S outperforms the recent VoxFormer by 2.2% points in mIoU but has a slightly lower IoU (-0.42% points). We explain that VoxFormer adopted a two-stage training approach, and the first stage was trained offline with temporal inputs, helping enhance occupancy precision. However, our SGN-S is end-to-end trained with only a single frame as input. Compared to the two-stage VoxFormer,

Method	IoU	road (15.30%)	sidewalk (11.13%)	parking (1.12%)	otherground (0.56%)	building (4.1%)	car (3.92%)	truck (0.16%)	bicycle (0.03%)	motorcycle (0.03%)	othervehicle (0.20%)	vegetation (30.3%)	trunk (0.51%)	terrain (9.17%)	person (0.07%)	bicyclist (0.07%)	motorcyclist (0.05%)	fence (3.90%)	pole (0.29%)	trafficsign (0.08%)	mIoU
LMSCNet <sup>†</sup> (Roldão, de Charette, and Verroust-Blondet 2020)	31.38	46.70	19.50	13.50	3.10	10.30	14.30	0.30	0.00	0.00	0.00	10.80	0.00	10.40	0.00	0.00	0.00	5.40	0.00	0.00	7.07
AICNet <sup>†</sup> (Li et al. 2020)	23.93	39.30	18.30	19.80	1.60	9.60	15.30	0.70	0.00	0.00	0.00	9.60	1.90	13.50	0.00	0.00	0.00	5.00	0.10	0.00	7.09
JS3C-Net <sup>†</sup> (Yan et al. 2021)	34.00	47.30	21.70	19.90	2.80	12.70	20.10	0.80	0.00	0.00	4.10	14.20	3.10	12.40	0.00	0.20	0.20	8.70	1.90	0.30	8.97
MonoScene (Cao and de Charette 2022)	34.16	54.70	27.10	24.80	5.70	14.40	18.80	3.30	0.50	0.70	<u>4.40</u>	14.90	2.40	19.50	1.00	1.40	<u>0.40</u>	11.10	3.30	2.10	11.08
TPVFormer (Huang et al. 2023)	34.25	55.10	27.20	27.40	6.50	14.80	19.20	<u>3.70</u>	1.00	0.50	2.30	13.90	2.60	20.40	1.10	2.40	0.30	11.00	2.90	1.50	11.26
VoxFormer (Li et al. 2023d)	42.95	53.90	25.30	21.10	5.60	19.80	20.80	3.50	1.00	0.70	3.70	22.40	7.50	21.30	1.40	<b>2.60</b>	0.20	11.10	5.10	4.90	12.20
OccFormer (Zhang, Zhu, and Du 2023)	34.53	55.90	<u>30.30</u>	<b>31.50</b>	6.50	15.70	21.60	1.20	1.50	<b>1.70</b>	3.20	16.80	3.90	21.30	<b>2.20</b>	1.10	0.20	11.90	3.80	3.70	12.32
SurroundOcc (Wei et al. 2023)	34.72	56.90	28.30	<u>30.20</u>	<u>6.80</u>	15.20	20.60	1.40	<u>1.60</u>	1.20	<u>4.40</u>	14.90	3.40	19.30	1.40	2.00	0.10	11.30	3.90	2.40	11.86
Symphonize (Jiang et al. 2023)	41.07	55.70	26.80	25.30	4.90	21.30	22.10	1.90	<b>1.70</b>	1.30	<b>5.80</b>	22.90	8.20	19.50	<b>2.20</b>	1.30	<b>0.50</b>	13.10	6.80	5.80	13.02
SGN-S (ours)	41.88	57.80	29.20	27.70	5.20	23.90	24.90	2.70	0.40	0.30	4.00	24.20	10.00	25.80	1.10	<u>2.50</u>	0.30	14.20	7.40	4.40	14.01
SGN-L (ours)	<u>43.71</u>	<u>57.90</u>	29.70	25.60	5.50	<u>27.00</u>	<u>25.00</u>	1.50	0.90	0.70	3.60	<u>26.90</u>	<u>12.00</u>	<u>26.40</u>	0.60	0.30	0.00	<u>14.70</u>	<u>9.00</u>	<u>6.40</u>	<u>14.39</u>
SGN-T (ours)	<b>45.42</b>	<b>60.40</b>	<b>31.40</b>	28.90	<b>8.70</b>	<b>28.40</b>	<b>25.40</b>	<b>4.50</b>	0.90	<u>1.60</u>	3.70	<b>27.40</b>	<b>12.60</b>	<b>28.40</b>	0.50	0.30	0.10	<b>18.10</b>	<b>10.00</b>	<b>8.30</b>	<b>15.76</b>

Table 1: **Semantic Scene Completion on SemanticKITTI hidden test set.** <sup>†</sup> denotes the results provided by MonoScene (Cao and de Charette 2022). Bold and underline denote the best performance and the second-best performance, respectively.

Method	IoU	road (15.30%)	sidewalk (11.13%)	parking (1.12%)	otherground (0.56%)	building (4.1%)	car (3.92%)	truck (0.16%)	bicycle (0.03%)	motorcycle (0.03%)	othervehicle (0.20%)	vegetation (30.3%)	trunk (0.51%)	terrain (9.17%)	person (0.07%)	bicyclist (0.07%)	motorcyclist (0.05%)	fence (3.90%)	pole (0.29%)	trafficsign (0.08%)	mIoU
LMSCNet <sup>†</sup> (Roldão, de Charette, and Verroust-Blondet 2020)	28.61	40.68	18.22	4.38	0.00	10.31	18.33	0.00	0.00	0.00	0.00	13.66	0.02	20.54	0.00	0.00	0.00	1.21	0.00	0.00	6.70
AICNet <sup>†</sup> (Li et al. 2020)	29.59	43.55	20.55	11.97	0.07	12.94	14.71	4.53	0.00	0.00	0.00	15.37	2.90	28.71	0.00	0.00	0.00	2.52	0.06	0.00	8.31
JS3C-Net <sup>†</sup> (Yan et al. 2021)	38.98	50.49	23.74	11.94	0.07	15.03	24.65	4.41	0.00	0.00	6.15	18.11	4.33	26.86	0.67	0.27	0.00	3.94	3.77	1.45	10.31
MonoScene (Cao and de Charette 2022)	37.12	57.47	27.05	15.72	<b>0.87</b>	14.24	23.55	7.83	0.20	0.77	3.59	18.12	2.57	30.76	1.79	1.03	0.00	6.39	4.11	2.48	11.50
TPVFormer (Huang et al. 2023)	35.61	56.50	25.87	<b>20.60</b>	<u>0.85</u>	13.88	23.81	8.08	0.36	0.05	4.35	16.92	2.26	30.38	0.51	0.89	0.00	5.94	3.14	1.52	11.36
VoxFormer (Li et al. 2023d)	44.02	54.76	26.35	15.50	0.70	17.65	25.79	5.63	0.59	0.51	3.77	24.39	5.08	29.96	1.78	<u>3.32</u>	0.00	7.64	7.11	4.18	12.35
OccFormer (Zhang, Zhu, and Du 2023)	36.50	58.85	26.88	19.61	0.31	14.40	25.09	<b>25.53</b>	<b>0.81</b>	<u>1.19</u>	8.52	19.63	3.93	32.62	<u>2.78</u>	2.82	0.00	5.61	4.26	2.86	13.46
Symphonize (Jiang et al. 2023)	41.44	55.78	26.77	14.57	0.19	18.76	27.23	<u>15.99</u>	<b>1.44</b>	<b>2.28</b>	<u>9.52</u>	24.50	4.32	28.49	<b>3.19</b>	<b>8.09</b>	0.00	6.18	8.99	5.39	13.44
SGN-S (ours)	43.60	<b>59.32</b>	<b>30.51</b>	18.46	0.42	21.43	31.88	13.18	0.58	0.17	5.68	25.98	7.43	34.42	1.28	1.49	0.00	<u>9.66</u>	9.83	4.71	14.55
SGN-L (ours)	<u>45.45</u>	59.00	<u>30.11</u>	19.35	0.21	<u>23.95</u>	<u>32.51</u>	9.74	0.39	0.15	5.19	<u>28.29</u>	<u>8.48</u>	<u>34.91</u>	0.78	0.20	0.00	8.83	<u>12.13</u>	<u>6.95</u>	<u>14.80</u>
SGN-T (ours)	<b>46.21</b>	<u>59.10</u>	29.41	19.05	0.33	<b>25.17</b>	<b>33.31</b>	6.03	0.61	0.46	<b>9.84</b>	<b>28.93</b>	<b>9.58</b>	<b>38.12</b>	0.47	0.10	0.00	<b>9.96</b>	<b>13.25</b>	<b>7.32</b>	<b>15.32</b>

Table 2: **Semantic Scene Completion on SemanticKITTI val set.** <sup>†</sup> denotes the results provided by MonoScene.

Variants	MSSD	SG	GG	VA GP	OA	IoU (%)	mIoU (%)
baseline						41.76	10.62
1	✓					43.22	13.00
2	✓	✓				43.32	13.68
3	✓	✓	✓			43.45	13.44
4	✓	✓	✓	✓		43.14	14.39
5	✓	✓	✓	✓	✓	<b>43.60</b>	<b>14.55</b>

Table 3: Ablation on network components

the higher mIoU score of our end-to-end SGN-S for semantic scene completion demonstrates the superiority of our framework of semantic propagation based on geometry prior and occupancy information.

Remarkably, our light version SGN-L achieves notable performance (45.45 IoU and 15.32 mIoU) on SemanticKITTI validation with only **12.5M** parameters. Compared with MonoScene, OccFormer, and VoxFormer with  $\sim 150M$ ,  $\sim 200M$ , and  $\sim 60M$  parameters, our SGN-L performs better while being more lightweight. It demonstrates that our

Methods	Mode	IoU (%)	mIoU (%)	Params (M)	Memory (G)
VoxFormer-S	two-stage	44.02	12.35	57.90	14.41
VoxFormer-T	two-stage	44.15	13.35	57.90	16.38
SGN-S (ours)	two-stage	<b>44.76</b>	<b>14.93</b>	<b>27.79</b>	<b>10.92</b>
SGN-S (ours)	one-stage	43.60	14.55	28.16	14.21
SGN-L (ours)	one-stage	45.45	14.80	<b>12.50</b>	<b>7.16</b>
SGN-T (ours)	one-stage	<b>46.21</b>	<b>15.32</b>	28.16	15.83

Table 4: Impact of different training modes. Memory denotes training memory

SGN requires no heavy 3D model and has a more powerful representation ability.

### Ablation studies

We do ablation studies on network components, training mode, image features, view transformation, and seed voxels on SemanticKITTI validation. All experiments are conducted with our SGN-S by default.

Backbone	scales				IoU (%)	mIoU (%)	Params (M)
	4	8	16	32			
ResNet50	✓				43.10	13.85	<u>28.06</u>
		✓			42.92	14.26	28.09
			✓		<b>43.60</b>	<u>14.55</u>	28.16
				✓	43.36	14.20	28.29
ResNet18	✓	✓	✓	✓	42.86	<b>14.60</b>	28.96
ResNet18				✓	<u>43.57</u>	14.08	<b>15.73</b>

Table 5: Ablation on image features

Module	IoU (%)	mIoU (%)	Params (M)	Memory (G)
FLoSP	<u>43.60</u>	<u>14.55</u>	<b>28.16</b>	<u>14.21</u>
LSS	42.95	<b>14.77</b>	30.56	<b>13.23</b>
Cross-Attention	<b>43.66</b>	14.05	62.15	19.01

Table 6: Ablation on view transformation. Memory denotes training memory

**Ablation on network components.** We do ablation studies to analyze the effect of the proposed semantic guidance (SG), geometry guidance (GG), multi-scale semantic diffusion (MSSD), and voxel aggregation layer (VA) in Table 3. GP and OA denote geometry prior and occupancy-aware information, respectively. Firstly, we construct a baseline that directly attaches a segmentation head after the selected seed features. As shown in the first line of Table 3, the constructed baseline has already achieved 41.76% IoU and 10.62% mIoU scores, demonstrating our depth-based sparse voxel proposal network can provide effective seed voxels. When equipped with our MSSD (Variant 1), the IoU and mIoU scores are improved by 1.46% points and 2.38% points, respectively. It demonstrates the effectiveness of multi-scale information propagation. And our semantic guidance on the seed features further boosts the mIoU by 0.68% points (Variant 2 vs. Variant 1), showing the importance of intra-category separation of seed features. On the other hand, the geometry guidance brings slight improvement in terms of IoU score, while the geometry prior further boosts the mIoU score by 0.95% points (Variant 4 vs. Variant 3). Besides, introducing occupancy-aware information can help improve performance (Variant 5 vs Variant 4). And comparing Variant 5 with Variant 1, the mIoU score is significantly boosted (+1.55% points), demonstrating the effectiveness of our semantic diffusion based on geometry prior and occupancy information.

**Impact of different training modes.** To explore the effect of different training modes, i.e., two-stage and one-stage training, we provide the detailed comparison results with VoxFormer in Table 4. Line 3 of Table 4 presents the results of our SGN-S with the two-stage training strategy. Note that when equipping SGN-S with a two-stage approach, the first stage remains the same as VoxFormer, and the parameters and training memory of the second stage are calculated for a fair comparison. In the same training configuration, Our SGN-S surpasses VoxFormer-S by a large margin regarding mIoU scores (+2.58% points). Even our one-stage SGN-S outperforms two-stage VoxFormer-S by 2.2% points in mIoU.

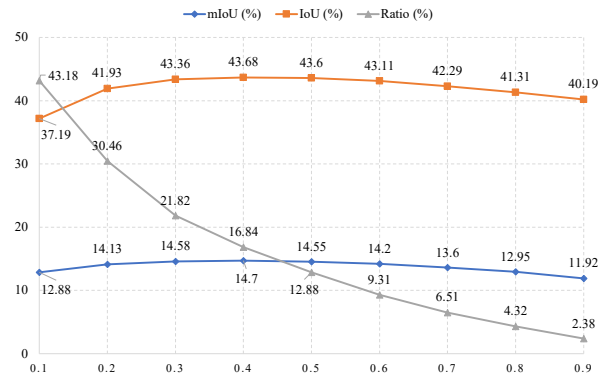


Figure 4: Impact of threshold values for seed voxels.

It is worth noting that the model parameters of our SGN-S are only about half of those of VoxFormer-S. For the temporal version, our SGN-T achieves 46.21 IoU and 15.32 mIoU scores, boosting VoxFormer-T by 2.06% points in IoU and 1.97% points in mIoU. Our light version, SGN-L, with only 12.5M parameters, also outperforms VoxFormer-T on mIoU and IoU scores while requiring only about half the training memory (7.16 G).

**Impact of image features.** The 2D features provide a foundation for informative voxel features. We do detailed experiments in Table 5 to explore the impact of the feature scale and image backbone. We see that using 2D features at a scale of 1/16 in ResNet 50 achieves the best IoU score and has comparable mIoU to other variants. And it strikes a balance between performance and model size. The results of using ResNet18 as the backbone are presented in the last line of Table 5 and shows that a lighter image backbone reduces the model parameters by 12.43M while the performance of the mIoU score drops by 0.47% points.

**Ablation on view transformation.** The view transformation generates the initial 3D features for the subsequent hybrid guidance and informative voxel features. We further investigate the effect of different view transformation modules. We implement three commonly used modules, i.e., FLoSP in Monoscene, LSS (Phillion and Fidler 2020), and cross-attention adopted from VoxFormer. The results are shown in Table 6, showing that using FLoSP contains fewer parameters while achieving comparable performance to other variants on both mIoU and IoU scores. Therefore, our SGN lifts the 2D features to 3D volume with the view transformation designed in the spirit of FLoSP.

**Exploration on the threshold for seed voxels.** We change the value  $\theta$  to investigate the impact of different thresholds for selecting seed voxels. We calculate the average occupancy rate of seed voxels, mIoU score, and IoU score for variants with  $\theta$  from 0.1 to 0.9. The results are shown in Figure 4, showing that the performance of the model first increases and then decreases as  $\theta$  increases. And when  $\theta = 0.4$ , the model achieves the best performance on both mIoU and IoU scores. Interestingly, we found our model still achieves notable mIoU and IoU scores when the occupancy ratio of the seed voxels is

very low ( $< 5\%$  points). It shows that seed voxels with high confidence play an essential role in our semantic diffusion.

## Conclusion

This work focuses on camera-based semantic scene completion (SSC). Existing methods usually rely on sophisticated 3D models to directly process the coarse lifted 3D features that are not discriminative enough for clear segmentation boundaries. Therefore, we propose the end-to-end SGN to diffuse semantics from the semantic- and occupancy-aware seed voxels to the whole scene based on geometry prior and occupancy information. By designing hybrid guidance and effective voxel aggregation, we enhance the intra-category feature separations and expedite the convergence of semantic diffusion. Extensive experiments on the SemanticKITTI benchmark demonstrate the effectiveness of Our SGN achieves state-of-the-art performance while being more lightweight.

## References

- Behley, J.; Garbade, M.; Milioto, A.; Quenzel, J.; Behnke, S.; Stachniss, C.; and Gall, J. 2019. SemanticKITTI: A dataset for semantic scene understanding of lidar sequences. In *Proceedings of the IEEE International Conference on Computer Vision*, 9297–9307.
- Berman, M.; Rannen Triki, A.; and Blaschko, M. B. 2018. The lovasz-softmax loss: A tractable surrogate for the optimization of the intersection-over-union measure in neural networks. In *Proceedings of the IEEE Conference on Computer Vision and Pattern Recognition*, 4413–4421.
- Cao, A.-Q.; and de Charette, R. 2022. Monoscene: Monocular 3d semantic scene completion. In *Proceedings of the IEEE/CVF Conference on Computer Vision and Pattern Recognition*, 3991–4001.
- Chen, S.; Cheng, T.; Wang, X.; Meng, W.; Zhang, Q.; and Liu, W. 2022a. Efficient and robust 2d-to-bev representation learning via geometry-guided kernel transformer. *arXiv preprint arXiv:2206.04584*.
- Chen, S.; Wang, X.; Cheng, T.; Zhang, Q.; Huang, C.; and Liu, W. 2022b. Polar parametrization for vision-based surround-view 3d detection. *arXiv preprint arXiv:2206.10965*.
- Cheng, R.; Agia, C.; Ren, Y.; Li, X.; and Bingbing, L. 2021. S3cnet: A sparse semantic scene completion network for lidar point clouds. In *Conference on Robot Learning*, 2148–2161. PMLR.
- Gan, W.; Mo, N.; Xu, H.; and Yokoya, N. 2023. A Simple Attempt for 3D Occupancy Estimation in Autonomous Driving. *arXiv preprint arXiv:2303.10076*.
- Geiger, A.; Lenz, P.; and Urtasun, R. 2012. Are we ready for autonomous driving? the kitti vision benchmark suite. In *2012 IEEE conference on computer vision and pattern recognition*, 3354–3361. IEEE.
- He, K.; Zhang, X.; Ren, S.; and Sun, J. 2016. Deep residual learning for image recognition. In *Proceedings of the IEEE conference on computer vision and pattern recognition*, 770–778.
- Huang, J.; Huang, G.; Zhu, Z.; Ye, Y.; and Du, D. 2021. Bevdet: High-performance multi-camera 3d object detection in bird-eye-view. *arXiv preprint arXiv:2112.11790*.
- Huang, Y.; Zheng, W.; Zhang, Y.; Zhou, J.; and Lu, J. 2023. Tri-perspective view for vision-based 3d semantic occupancy prediction. In *Proceedings of the IEEE/CVF Conference on Computer Vision and Pattern Recognition*, 9223–9232.
- Jiang, H.; Cheng, T.; Gao, N.; Zhang, H.; Liu, W.; and Wang, X. 2023. Symphonize 3D Semantic Scene Completion with Contextual Instance Queries. *arXiv preprint arXiv:2306.15670*.
- Li, B.; Sun, Y.; Jin, X.; Zeng, W.; Zhu, Z.; Wang, X.; Zhang, Y.; Okae, J.; Xiao, H.; and Du, D. 2023a. StereoScene: BEV-Assisted Stereo Matching Empowers 3D Semantic Scene Completion. *arXiv preprint arXiv:2303.13959*.
- Li, J.; Han, K.; Wang, P.; Liu, Y.; and Yuan, X. 2020. Anisotropic convolutional networks for 3d semantic scene completion. In *Proceedings of the IEEE/CVF Conference on Computer Vision and Pattern Recognition*, 3351–3359.
- Li, P.; Zhao, R.; Shi, Y.; Zhao, H.; Yuan, J.; Zhou, G.; and Zhang, Y.-Q. 2023b. Lode: Locally conditioned eikonal implicit scene completion from sparse lidar. *arXiv preprint arXiv:2302.14052*.
- Li, Y.; Li, S.; Liu, X.; Gong, M.; Li, K.; Chen, N.; Wang, Z.; Li, Z.; Jiang, T.; Yu, F.; et al. 2023c. SSCBench: A Large-Scale 3D Semantic Scene Completion Benchmark for Autonomous Driving. *arXiv preprint arXiv:2306.09001*.
- Li, Y.; Yu, Z.; Choy, C.; Xiao, C.; Alvarez, J. M.; Fidler, S.; Feng, C.; and Anandkumar, A. 2023d. Voxformer: Sparse voxel transformer for camera-based 3d semantic scene completion. In *Proceedings of the IEEE/CVF Conference on Computer Vision and Pattern Recognition*, 9087–9098.
- Li, Z.; Wang, W.; Li, H.; Xie, E.; Sima, C.; Lu, T.; Qiao, Y.; and Dai, J. 2022. Bevformer: Learning bird’s-eye-view representation from multi-camera images via spatiotemporal transformers. In *European conference on computer vision*, 1–18. Springer.
- Li, Z.; Yu, Z.; Austin, D.; Fang, M.; Lan, S.; Kautz, J.; and Alvarez, J. M. 2023e. FB-OCC: 3D Occupancy Prediction based on Forward-Backward View Transformation. *arXiv preprint arXiv:2307.01492*.
- Lin, T.-Y.; Dollár, P.; Girshick, R.; He, K.; Hariharan, B.; and Belongie, S. 2017. Feature pyramid networks for object detection. In *Proceedings of the IEEE conference on computer vision and pattern recognition*, 2117–2125.
- Liu, Y.; Wang, T.; Zhang, X.; and Sun, J. 2022. Petr: Position embedding transformation for multi-view 3d object detection. In *European Conference on Computer Vision*, 531–548. Springer.
- Loshchilov, I.; and Hutter, F. 2017. Decoupled weight decay regularization. *arXiv preprint arXiv:1711.05101*.
- Mei, J.; Yang, Y.; Wang, M.; Huang, T.; Yang, X.; and Liu, Y. 2023. SSC-RS: Elevate LiDAR Semantic Scene Completion with Representation Separation and BEV Fusion. *arXiv preprint arXiv:2306.15349*.



- Miao, R.; Liu, W.; Chen, M.; Gong, Z.; Xu, W.; Hu, C.; and Zhou, S. 2023. Occdepth: A depth-aware method for 3d semantic scene completion. *arXiv preprint arXiv:2302.13540*.
- Phillion, J.; and Fidler, S. 2020. Lift, splat, shoot: Encoding images from arbitrary camera rigs by implicitly unprojecting to 3d. In *Computer Vision–ECCV 2020: 16th European Conference, Glasgow, UK, August 23–28, 2020, Proceedings, Part XIV 16*, 194–210. Springer.
- Rist, C. B.; Emmerichs, D.; Enzweiler, M.; and Gavrilu, D. M. 2021. Semantic scene completion using local deep implicit functions on lidar data. *IEEE transactions on pattern analysis and machine intelligence*, 44(10): 7205–7218.
- Roldão, L.; de Charette, R.; and Verroust-Blondet, A. 2020. LMSCNet: Lightweight Multiscale 3D Semantic Completion. In *3DV 2020-International Virtual Conference on 3D Vision*.
- Shamsafar, F.; Woerz, S.; Rahim, R.; and Zell, A. 2022. Mobilestereonet: Towards lightweight deep networks for stereo matching. In *Proceedings of the IEEE/CVF Winter Conference on Applications of Computer Vision*, 2417–2426.
- Song, S.; Yu, F.; Zeng, A.; Chang, A. X.; Savva, M.; and Funkhouser, T. 2017. Semantic scene completion from a single depth image. In *Proceedings of the IEEE Conference on Computer Vision and Pattern Recognition*, 1746–1754.
- Tian, X.; Jiang, T.; Yun, L.; Wang, Y.; Wang, Y.; and Zhao, H. 2023. Occ3d: A large-scale 3d occupancy prediction benchmark for autonomous driving. *arXiv preprint arXiv:2304.14365*.
- Wang, T.; Zhu, X.; Pang, J.; and Lin, D. 2021. Fcos3d: Fully convolutional one-stage monocular 3d object detection. In *Proceedings of the IEEE/CVF International Conference on Computer Vision*, 913–922.
- Wang, X.; Zhu, Z.; Xu, W.; Zhang, Y.; Wei, Y.; Chi, X.; Ye, Y.; Du, D.; Lu, J.; and Wang, X. 2023. Openoccupancy: A large scale benchmark for surrounding semantic occupancy perception. *arXiv preprint arXiv:2303.03991*.
- Wang, Y.; Guizilini, V. C.; Zhang, T.; Wang, Y.; Zhao, H.; and Solomon, J. 2022. Detr3d: 3d object detection from multi-view images via 3d-to-2d queries. In *Conference on Robot Learning*, 180–191. PMLR.
- Wei, Y.; Zhao, L.; Zheng, W.; Zhu, Z.; Zhou, J.; and Lu, J. 2023. Surroundocc: Multi-camera 3d occupancy prediction for autonomous driving. *arXiv preprint arXiv:2303.09551*.
- Xia, Z.; Liu, Y.; Li, X.; Zhu, X.; Ma, Y.; Li, Y.; Hou, Y.; and Qiao, Y. 2023. SCPNet: Semantic Scene Completion on Point Cloud. In *Proceedings of the IEEE/CVF Conference on Computer Vision and Pattern Recognition*, 17642–17651.
- Yan, X.; Gao, J.; Li, J.; Zhang, R.; Li, Z.; Huang, R.; and Cui, S. 2021. Sparse single sweep lidar point cloud segmentation via learning contextual shape priors from scene completion. In *Proceedings of the AAAI Conference on Artificial Intelligence*, volume 35, 3101–3109.
- Yang, X.; Zou, H.; Kong, X.; Huang, T.; Liu, Y.; Li, W.; Wen, F.; and Zhang, H. 2021. Semantic segmentation-assisted scene completion for lidar point clouds. In *2021 IEEE/RSJ International Conference on Intelligent Robots and Systems (IROS)*, 3555–3562. IEEE.
- Ye, M.; Wan, R.; Xu, S.; Cao, T.; and Chen, Q. 2022. Efficient Point Cloud Segmentation with Geometry-Aware Sparse Networks. In *Computer Vision–ECCV 2022: 17th European Conference, Tel Aviv, Israel, October 23–27, 2022, Proceedings, Part XXXIX*, 196–212. Springer.
- Ye, M.; Xu, S.; Cao, T.; and Chen, Q. 2021. Drinet: A dual-representation iterative learning network for point cloud segmentation. In *Proceedings of the IEEE/CVF international conference on computer vision*, 7447–7456.
- Zhang, J.; Zhao, H.; Yao, A.; Chen, Y.; Zhang, L.; and Liao, H. 2018. Efficient semantic scene completion network with spatial group convolution. In *Proceedings of the European Conference on Computer Vision (ECCV)*, 733–749.
- Zhang, Y.; Zhu, Z.; and Du, D. 2023. OccFormer: Dual-path Transformer for Vision-based 3D Semantic Occupancy Prediction. *arXiv preprint arXiv:2304.05316*.
- Zhou, B.; and Krähenbühl, P. 2022. Cross-view transformers for real-time map-view semantic segmentation. In *Proceedings of the IEEE/CVF conference on computer vision and pattern recognition*, 13760–13769.
- Zhou, H.; Zhu, X.; Song, X.; Ma, Y.; Wang, Z.; Li, H.; and Lin, D. 2020. Cylinder3D: An Effective 3D Framework for Driving-scene LiDAR Semantic Segmentation. *arXiv preprint arXiv:2008.01550*.
- Zou, H.; Yang, X.; Huang, T.; Zhang, C.; Liu, Y.; Li, W.; Wen, F.; and Zhang, H. 2021. Up-to-Down Network: Fusing Multi-Scale Context for 3D Semantic Scene Completion. In *2021 IEEE/RSJ International Conference on Intelligent Robots and Systems (IROS)*, 16–23. IEEE.

Methods	Modality	IoU (%)			mIoU (%)		
		12.8m	25.6m	51.2m	12.8m	25.6m	51.2m
SSCNet (Song et al. 2017)	LiDAR	64.37	61.02	<u>50.22</u>	20.02	19.68	<u>16.35</u>
JS3CNet (Yan et al. 2021)	LiDAR	63.47	<b>63.40</b>	<b>53.09</b>	<b>30.55</b>	<b>28.12</b>	<b>22.67</b>
MonoScene* (Cao and de Charette 2022)	Camera	38.42	38.55	36.80	12.25	12.22	11.30
OccFormer (Zhang, Zhu, and Du 2023)	Camera	56.38	47.28	36.50	20.91	17.90	13.46
VoxFormer-T (Li et al. 2023d)	Camera	65.38	57.69	44.15	21.55	18.42	13.35
SGN-S (ours)	Camera	64.21	56.20	43.60	21.53	19.60	14.55
SGN-L (ours)	Camera	<u>70.08</u>	61.17	45.45	24.76	21.17	14.80
SGN-T (ours)	Camera	<b>70.61</b>	<u>61.90</u>	46.21	<u>25.70</u>	<u>22.02</u>	15.32

Table 7: **Quantitative comparison** in different ranges. “\*” denotes the results provided by VoxFormer.

## Appendix

### Dataset and Metrics

**Dataset.** For large-scale outdoor scene understanding, the KITTI odometry dataset (Geiger, Lenz, and Urtasun 2012) collects 22 sequences with 20 classes with a Velodyne HDL-64 laser scanner in the scenes of autonomous driving. SemanticKITTI (Behley et al. 2019) is based on the KITTI dataset and provides semantic annotation of all sequences. According to the official setting for semantic scene completion (SSC), sequences 00-07 and 09-10 (a total of 3834 scans) are for training, sequence 08 (815 scans) is for validation, and the rest (3901 scans) is for testing. The volume of interest for the SSC benchmark is  $[0 \sim 51.2m, -25.6m \sim 25.6m, -2 \sim 4.4m]$ , and the voxelization resolution  $s$  is  $0.2m$ . The SSC labels with resolution  $256 \times 256 \times 32$  of train and validation set are provided for the users. In this work, we focus on the camera-based SSC, taking the RGB images as inputs similar to (Cao and de Charette 2022; Li et al. 2023d; Jiang et al. 2023).

**Metrics.** Following (Song et al. 2017), we mainly report the Intersection-over-Union (IoU) for scene completion and mIoU of  $C_n = 19$  classes (no “unlabeled” class) for semantic scene completion. The mIoU is calculated by:

$$mIoU = \frac{1}{C_n} \sum_{c=1}^{C_n} \frac{TP_c}{TN_c + FP_c + FN_c} \quad (10)$$

where  $TP_c$ ,  $TN_c$ ,  $FP_c$ , and  $FN_c$  denote true positive, true negative, false positive, and false negative for class  $c$ .

### Further Analysis

We conduct a series of experiments on SemanticKITTI validation to provide further analysis on ranges, model dimensions, and temporal input. The efficiency analysis is also provided.

**Quantitative comparison in different ranges.** We also provide the results of different ranges in Table 7. The results show that SGN-T achieves mIoU scores of 25.70% and 22.02% within 12.8 meters and 25.6 meters and performs better than VoxFormer-T by 4.15% and 3.60% points in mIoU, respectively. Additionally, our SGN-S surpassed MonoScene by 9.28% and 7.38% points in mIoU within 12.8 meters and 25.6 meters. Notably, SGN-T obtains competitive performance with LiDAR-based methods in short-range (12.8

Dimensions	Depth	IoU (%)	mIoU (%)	Params (M)	Memory (G)
64	1	43.16	<b>14.24</b>	<b>24.88</b>	<b>7.23</b>
64	2	<b>43.73</b>	14.17	<u>24.93</u>	<u>7.27</u>
64	3	<u>43.32</u>	<u>14.20</u>	24.97	8.04
128	3	<b>43.60</b>	<b>14.55</b>	28.16	14.21

Table 8: Number of model dimensions and depth of MSSD. Memory denotes training memory

Frames	IoU (%)	mIoU (%)	Memory (G)
1	43.60	14.55	<b>14.21</b>
2	44.39	15.36	<u>14.71</u>
3	45.50	<b>15.75</b>	15.19
4	<u>45.84</u>	<u>15.56</u>	15.67
5	<b>46.21</b>	15.32	15.83
6	45.65	15.29	16.59
7	45.55	15.34	17.97

Table 9: Effect of temporal frames.

meters) areas. For example, SGN-T outperforms SSCNet by 5.58% points in mIoU and 6.24% points in IoU within 12.8 meters, demonstrating the effectiveness of our camera-based method for autonomous driving.

**Number of model dimensions.** The impact of the number of model dimensions of our SGN-S is evaluated and presented in Table 8. The results reveal that using a large number of feature channels for 3D features boosts the models’ performance while increasing the model complexity. For example, the model with 64 dimensions contains fewer parameters and requires less training memory, although its performance drops by 0.28% points in IoU and 0.35% points in mIoU (Line3 vs Line4). We also provide the results of different depths for the multi-scale semantic diffusion module. We see that using different depths has comparable mIoU and IoU, demonstrating that our model with hybrid guidance and semantic diffusion avoids the dependency on the heavy 3D model for processing 3D features.

**Effect of temporal input.** Finally, we explore the impact of the number of temporal frames in Table 9. We take historical frames to form the temporal input. As Table 9 shows, the model’s performance on IoU scores first increases with the number of frames and then decreases. We explain that the camera extrinsic matrix from the historical frame to the current system is not always accurate, especially when the temporal interval is long. Therefore, the 3D points may project on the wrong image patches of the historical frames, which disturbs the learning of voxel features.

**Efficiency analysis.** We perform runtime experiments on a single V100 GPU. The mean value over the SemanticKITTI test set is reported. Our SGN-S, SGN-L, and SGN-T run in 327.71 ms, 315.35 ms, and 436.24 ms, respectively. We also tested the recent VoxFormer-T (261.46 ms) and OccFormer (322.87 ms) on the same platform with the officially provided weights for a fair comparison. Compared with these methods, our light version SGN-L has comparable latency but better

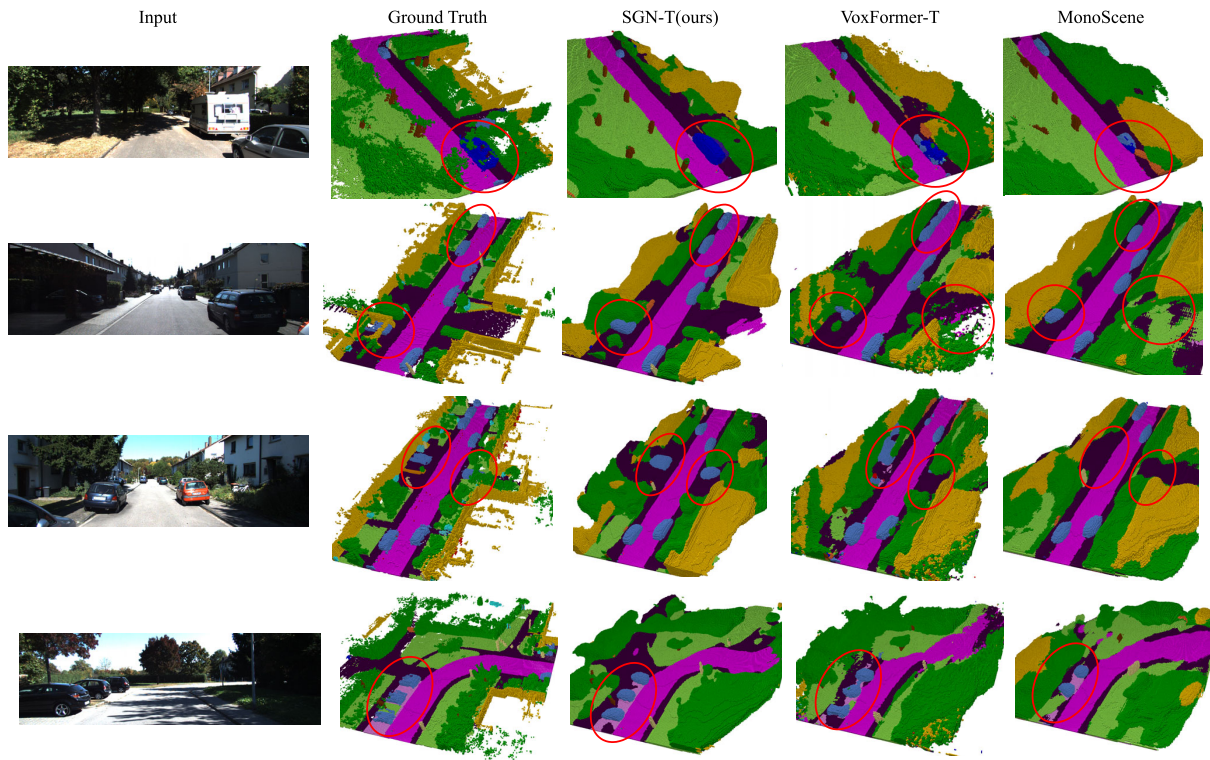


Figure 5: Visual comparison of our SGN-T with state-of-the-art methods on SemanticKITTI validation. Compared to VoxFormer-T and MonoScene, our SGN-T generates more precise segmentation boundaries . (labeled in red circles).

applicability due to its lightweight (12.5M parameters) and less training memory consumption (7.16 G).

### Qualitative Visualizations

We provide the visualization results of the proposed SGN-T on SemanticKITTI validation in Fig. 5. Compared to VoxFormer-T and MonoScene, our SGN-T generates more precise segmentation boundaries, especially on “plane” classes and large objects such as cars. Besides, SGN-T predicts more accurate SSC results and preserves more regional details in the short-range areas than other methods. For example, there are some wrong semantics and missing objects for VoxFormer-T and MonoScene in the short-range areas, as shown in the first and third rows in Fig. 5. However, we noticed that our SGN-T also missed some distant objects that are very small in RGB images. We explain that our SGN uses image features of the 1/16 scale, which may degrade the performance of objects in distant areas.